JOURNAL OF MATERIALS SCIENCE 26 (1991) 3292–3304

A study on an atomized Al–Fe–Mo–Zr powder to be processed for high temperature applications

J. ZHOU, J. DUSZCZYK, B. M. KOREVAAR
Laboratory for Materials Science, Delft University of Technology, Rotterdamseweg 137, 2628 AL Delft, The Netherlands

The performance of a powder metallurgy material in processing and service depends very much upon the initial characteristics of the atomized powder. An investigation on the characterization of an Al–8.5Fe–2Mo–1Zr alloy powder, to be further processed for high temperature applications, has, therefore, been carried out. Analyses have been performed of its composition, morphology, size and microstructure by means of chemical and metallographic methods. Results show that although the powder was atomized in nitrogen, its oxide and hydrogen contents are high enough to be comparable to those of other aluminium alloy powders atomized in air. Auger spectroscopy indicates the presence of discrete oxide particles at a depth of 100 nm below the powder particle surface, which corresponds to the topography of the powder particles revealed by SEM. The oxidation during atomization, plus further oxidation and moisture adsorption during subsequent handling, is considered to be mainly responsible for the analysed results, in addition to the contributing factor that the present powder has a relatively high specific surface area. Applying an appropriate degassing process is, therefore, of particular importance for obtaining the desired properties of the material processed from the powder. In order to simplify the process and to minimize the coarsening of microstructure, an on-line degassing technique has been proposed. X-ray diffractometry shows that the lattice parameter of the α-Al matrix in the present powder is altered in a complicated way, and that the diffraction spectrum of intermetallic particles does not match any established phase, presumably due to the involvement of molybdenum in a metastable phase to form an Al–Fe–Mo intermetallic. The microstructure of the powder particles finer than 10 μm is featureless, and larger ones exhibit a distinctive microstructure which is composed of a featureless zone, a transitional zone and a cellular zone. The relative percentage of the three zones is strongly dependent upon the size of individual powder particles and thus their cooling rates. Solidification processes responsible for the formation of the three zones are described in this paper. It is also found that as a result of microstructural inhomogeneity, microhardness within and between the powder particles differs significantly, and this difference can be retained after consolidation and influence the properties of the final engineering material. It is thus thought that creating an extremely fine powder particle size (smaller than 10 μm) with an overwhelming featureless microstructure may not be commercially feasible at present, while producing a fairly homogeneous microstructure by narrowing the scattering range of powder particle size could be more important for obtaining uniform deformation and oxide break-up during consolidation, and desired mechanical properties of the final product.

1. Introduction

Aluminium alloys with an adequate strength at elevated temperatures are increasingly demanded in structural applications. Unfortunately, the thermal stability of aluminium alloys presently in use, mostly produced in a conventional way, is not satisfactory [1]. The improvement of their hot strength through heavy alloying is, however, restricted by macrosegregation, and as a result titanium alloys have to be used in many applications instead. The recent introduction of rapid solidification has brought a breakthrough to the problem associated with alloying, which makes it possible to fabricate highly alloyed aluminium with a fine structure and desired mechanical properties. So far, several alloy systems designed for high temperature applications have appeared, of which rapidly solidified Al–Fe alloys or Al–Fe based ternary or quaternary alloys have received the most attention. An important finding on a microstructural transition in splat-quenched Al–Fe ribbons by Jones [2] has led to a number

0022–2461/91 $03.00 + .12

of studies on the structure of very thin, melt-spun ribbons of Al–Fe–X alloys [3–7]. Such a structural transition has, however, been claimed to be not as easily observed in atomized powders as in the ribbons with similar chemical compositions [8]. On the other hand, due to the recognition that powder metallurgy (PM) is the most suitable technique for bulk production of rapidly solidified materials [9], work on Al–Fe–X alloys prepared from atomized powder has been undertaken, but most of it is directed toward their final mechanical properties [10–18]. Systematic investigations on characterization of loose powders to be processed through consolidation to final engineering materials are lacking. The aim of the present work was to provide a comprehensive description of the characteristics of an Al–Fe–Mo–Zr powdered alloy which are expected to influence its fabrication behaviour and eventually mechanical properties.

2. Experimental procedure

The alloy, with a nominal composition of 8.5% Fe, 2.0% Mo, 1.0% Zr and balance Al, in the form of powder, was supplied by the Centre de Recherches de Voreppe S.A., France. The powder was produced in a pilot atomizer, and nitrogen was used as atomizing gas in an attempt to prevent severe oxidation and to obtain a regular shape of the atomized powder particles.

The as-received powder was first subjected to analysis of its composition, for which inductively coupled plasma (ICP) [19] was used as an emission source for spectroscopic analysis. A sample was prepared by mixing 0.5 g powder in a 20 ml HCl (1 : 1) solvent, and adding a few drops of H_2O_2 to oxidize the solution. The sample solution was then carried by argon to be introduced into a Perkin-Elmer Plasma-40 instrument. The ICP analysed result of the powdered alloy is presented in Table I, and compared with its nominal composition and that given by the supplier of the powder.

Oxygen and hydrogen contents, which are regarded as important characteristics of the powder in consideration of subsequent processing, were analysed separately. The measurement of the oxygen content was made by heating 0.04 g powder in the presence of carbon up to 1993 °C to reduce all kinds of oxides present in the powder, and then to determine the oxygen from the carbon monoxide formed [20]. Stroehlein OSAA–MAT 350 instrument was employed and argon used as carrier gas. The hydrogen content was measured using a Stroehlein H-Mat 251 gas analyser working in the hot extraction mode. 2.5 g powder was heated in an attached tilting furnace at 560 °C for 20 min, and nitrogen used as carrier gas. Analysis was done by comparing the difference in thermal conductivity between pure nitrogen and nitrogen plus hydrogen.

TABLE I Chemical composition of the atomized powder

	Fe	Mo	Zr	Si	Al
nominal	8.5	2.0	1.0	–	bal.
analysed by the supplier	9.0	2.3	1.0	0.2	bal.
analysed by the authors	9.48	1.86	0.80	0.21	bal.

To determine the in-depth distribution of the elements, the compositions at the surface and subsurface of the powder particles were analysed using an Auger spectrometer (Physical Electronics 545 AES system). Random powder particles were lightly pressed on an indium foil and loaded in the instrument. Composition profiles were obtained by successive ion etching for 10 min, during which analysis was done every half minute. Etching was performed at an accelerating voltage of 2 kV and with a beam diameter of about 15 μm, which corresponded to an approximate sputtering rate of 10 nm·min^{-1} for a given emission current.

The morphology of the powder was observed using optical and scanning electron microscopy (SEM). An optical specimen was prepared by mixing the powder particles in a mounting resin followed by polishing. For SEM observation, the powder particles were scattered evenly on a double sided tape and then covered by a gold layer. The size and size distribution of the powder were determined by means of a Malvern 2600 laser particle sizer. A representative quantity of the powder was blown into the instrument to create a Fraunhofer diffraction spectrum and its size was interpreted from the diffraction pattern. The specific surface area of the powder was measured using a gas adsorption method, named after Brunauer, Emmett, and Teller (BET) [21]. Krypton was applied as adsorbate to contact the surfaces of 0.56 g powder (adsorbent) and the specific surface area was calculated from the volume and relative pressure p/p^0 of the adsorbate over the range of 0.05 to 0.21, where p^0 is the saturation pressure of the pure adsorbate at the temperature of measurement and p is the pressure measured after adsorption.

The microstructural observation of the powder particle sections was made using a Neophot optical microscope. The specimen was etched in a diluted Keller's reagent or in a 0.5% HF solution. SEM (Jeol JXA 50A) operating over the voltage range of 10 to 25 kV was also performed to reveal the microstructures in secondary electron mode and back scattered electron mode. For this, the powder particles were first mounted in a copper-based resin, and the polished powder particle sections were deeply etched in the 0.5% HF solution, followed by depositing a carbon film. Lattice parameter determination and phase identification were made by using a Siemens D500B X-ray powder diffractometer. Cobalt radiation (50 kV–20 mA) was employed, and profiles were recorded by a preset time method. The powder particles were mixed in alcohol and deposited on a silicon monocrystal substrate with the orientation of ⟨5 1 0⟩. After alcohol evaporation, a very thin layer of the powder particles was attached to the substrate and loaded into the instrument to be analysed.

3. Results and discussion

3.1. Oxygen and hydrogen determination

3.1.1. Oxygen content

Fig. 1 shows the oxygen evolution spectrum of the powder heated over the temperature range of 950 to 1993 °C for about 160 s. The accumulated percentage of evolved oxygen was calculated to be 0.227% in weight, by integrating the area below the curve. This value is very high, being in the same range as that of the previously investigated Al–Si–X alloy powders atomized in air (between 0.20 and 0.22 wt %) [22]. It is clear that the oxygen content in a powder is mainly governed by the oxygen affinity of the elements present, the availability of oxygen during atomization and subsequent handling, and the specific surface area of the powder. For the present alloy, the elements involved in the powder lead to a strong tendency to oxidation. The possible contamination of the powder during atomization in nitrogen and subsequent handling, as will be discussed later, cannot, therefore, be ruled out.

The measurement of specific surface area of the present powder showed a value of 0.3090 $m^2 g^{-1}$, which is much higher than that of the above-mentioned, air-atomized Al–Si–X powders (0.17 $m^2 g^{-1}$ on average) and twice as high as that of an Al–Si–Fe–Ni alloy powder atomized in argon (0.16 $m^2 g^{-1}$) [22]. Although the specific surface area originally represents the amount of gas adsorbed in the monolayer of the powder particles, it equivalently reflects the exposed area potentially to be oxidized whenever possible. A higher value of specific surface area, due to finer powder particle sizes and less smooth surfaces, means a larger reactive surface area in unit weight. Characterizing this factor is of great importance, because it partially accounts for the relatively high oxide content in the present powder, but unfortunately, in most of the previous work on the characterization of powders, this factor is very often neglected. The present results indicate that many characteristics of powder particles are strongly related to each other, and it is difficult to make comparisons between powders merely on the bases of one or two characteristics.

3.1.2. Hydrogen content

The hydrogen content in the present powder was found to be 19.8 p.p.m. This value is close to that measured in an Al–Fe–Ce powder (17.5 p.p.m.) [23]. It is known that the oxides on aluminium powder particle surfaces are usually hygroscopic so that moisture can easily be picked up to form hydroxides during cooling after solidification if the dew point in an atomizing chamber is not low enough, and during post-atomization handling and storage if air insulation is inadequate. Aluminium is the strongest oxide former among the elements in the present aluminium-based alloy; thus we may reasonably assume that most of the oxides are Al_2O_3 and hydroxides are $Al_2O_3 \cdot xH_2O$, where x is between 1 and 3. According to the chemical formulae, the measured 19.8 p.p.m. hydrogen in the moisture is balanced with 316.8 p.p.m. oxygen and 633.6 p.p.m. oxygen in $Al_2O_3 \cdot 3H_2O$ and $Al_2O_3 \cdot 1H_2O$, respectively, while the measured oxygen content in the powder, as given earlier, is 2270 p.p.m. This means that only a part of the oxide present at the surface of the powder particles is hydrolysed.

The hydrogen present on the powder particle surface, if not eliminated, is a potential source of porosity in the material. When the contaminated powder is exposed to a temperature high enough to cause the decomposition of the hydroxides, which may be inevitable for the present highly alloyed aluminium powder in processing and service, the hydrogen will be evolved and as a consequence pressure built up to create porosity within the consolidated material or surface blistering. In the former case, the bonding between the powder particles will be severely weakened, which is particularly detrimental to the strength

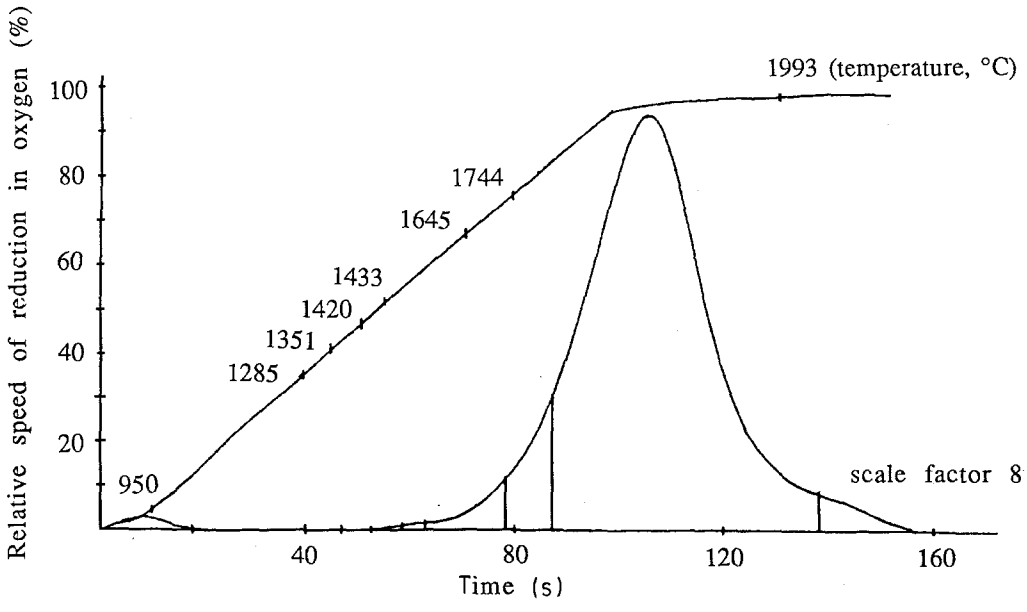

Figure 1 Oxygen evolution spectrum of the powder.

and ductility of the material. In the latter case, the surface quality will be spoiled. Moreover, it has been reported that a high hydrogen content in an Al–Fe–X powder leads to poor weldability of the final engineering material [24, 25]. The present work therefore underlines the importance of a degassing step in the fabrication cycle of this powdered alloy. During degassing, dehydration of $Al_2O_3 \cdot 3H_2O$ and evaporation of adsorbed H_2O–O_2 take place [26], so that the unfavourable effect of hydrogen can substantially be lessened. On the other hand, complete degassing gives rise not only to extra costs for material fabrication but also to coarsening of dispersed particles [23], which is obviously undesirable in view of the strength of the material. To make a compromise, it is therefore suggested to perform on-line degassing at a temperature somewhat higher than the maximum temperature that will possibly be used in subsequent processing and service, just prior to consolidation. The consolidation by hot extrusion should be carried out at a sufficiently high reduction ratio so that the tenacious oxide film on the powder particle surface can be broken up and the oxide particles in the subsurface can be redistributed. With this cost-effective technique, in addition to minimizing microstructural coarsening, reheating for hot extrusion can be avoided, and more importantly sealing cans and crimping evacuation tubes can be eliminated which are generally difficult to do securely.

3.2. Surface composition analysis

Fig. 2 shows a composition depth profile of the powder particles in atomic percentage, in which the relative concentrations of molybdenum and zirconium are too low to be given. It can be seen that at the top surface of the powder particles, the oxygen concentration is approximately 68 at %, below which it drops very quickly, being about halved after sputtering for half a minute. The average oxide thickness is thus approximately 5 nm, which is defined as the depth where the oxygen concentration has decreased by 50% [27]. This value is in good agreement with an estimate (5.18 nm), which was made from the measured oxygen content, specific surface area and density (about 3.0 $g\,cm^{-2}$ [28]) and on the assumption that the oxides are mostly present in the form of Al_2O_3 and that the oxygen in moisture is removed in the high vacuum system of the Auger instrument. It is of great importance to point out that the determined average oxide thickness does not mean that a 5 nm thick oxide layer uniformly covers the powder particles. Auger spectra obtained at 5 nm below the top surface revealed an oxygen concentration value, being half of that expected for Al_2O_3 (60 at %), and the presence of aluminium in the metallic state. This result is in accord with the findings on other aluminium alloy powders atomized in an inert atmosphere [29]. It clearly indicates that a continuous surface oxide film on the top surface of the powder particles is extremely thin (thinner than 5 nm), and below that film discrete oxides are present which only partially cover the powder particles.

At a depth of 5 nm, molybdenum and zirconium were not detectable. There is no reason to suggest a local depletion of these elements, because they both are also oxide formers. A possible explanation could be that the high percentage of oxygen there brought them just below the detecting limit. On further sputtering, their characteristic peaks became visible in the Auger spectra. With longer sputtering time, the concentrations of oxygen and aluminium kept changing slowly. Note that at a depth of 100 nm, the oxygen

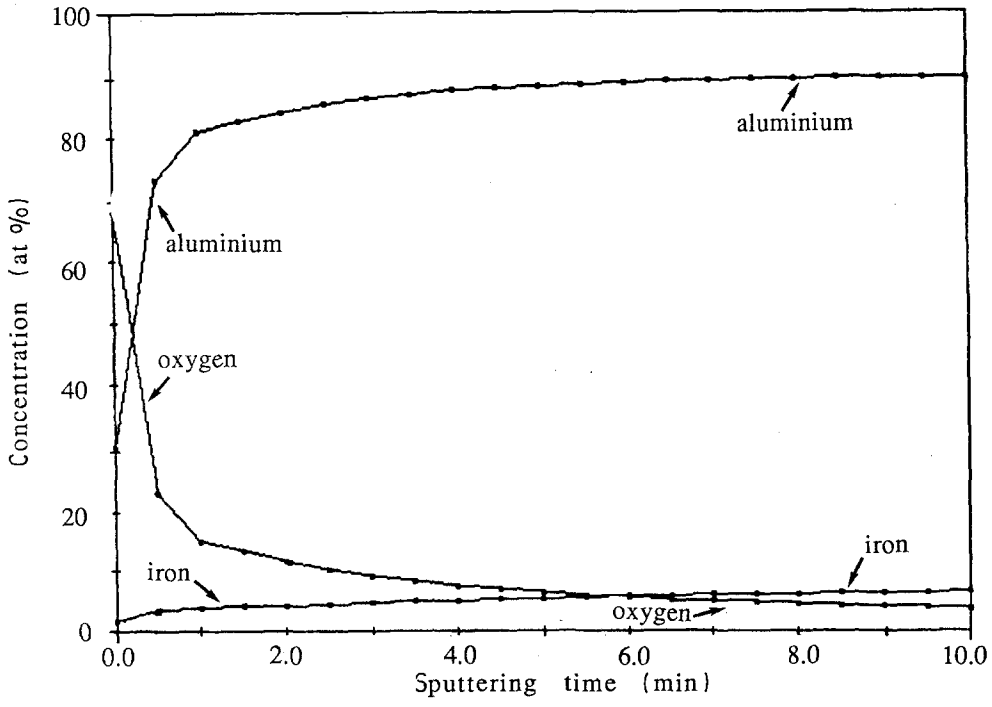

Figure 2 Depth profile of the powder showing the composition variation of aluminium, oxygen and iron in the 100 nm thick layer of powder particle surface.

concentration still holds a value of about 4 at %. It confirms that deep, discrete oxide particles do exist in the subsurface, being consistent with the observation of the powder particle surfaces by SEM, as will be discussed later. The results from the Auger analysis, together with the high value of specific surface area, account for the high oxygen content in the present powder, given earlier in this communication. The deep, discrete oxide particles are very unlikely to be formed at low temperatures where the oxidation would be fairly limited. In consideration of the kinetics of oxidation, over the usual temperature range of atomization, the equilibrium partial pressure of oxygen for the formation of aluminium oxides is as low as approximately 10^{-60} mbar [30]. Such a pure atmosphere is not easily obtainable. In practice, it is known that, as long as the oxygen concentration in an atomizing atmosphere is higher than 20 to 50 p.p.m., the oxidation of aluminium powders cannot be effectively prevented [31], in spite of the fact that the powder is cooled at a very high rate. For example, the average oxygen thickness in an argon atomized Al–Cr–Zr–Mn powder was found to be essentially the same as that in the air atomized [32]. It is, therefore, considered that most of the deep, discrete oxide particles in the present powder were mainly formed through the reactions between the residual oxygen in the atomizer and the strongest oxide former, aluminium, although it is also possible that a small amount of oxygen was dissolved in the melt. Further oxidation took place during subsequent handling and storage, resulting in the increased oxygen concentrations in the surface layer and a continuous oxide film with a thickness less than 5 nm, as typically happens to pure aluminium in air at room temperature [31].

3.3. Powder size and morphology

Fig. 3 shows the size distribution of the powder investigated, which was obtained by using non-linear least square analysis. The median diameter was calculated to be 30 μm. It can be seen from the figure that 90% of the powder particles are under the size of 60 μm and only 8% are under 10 μm. It is clear that the smaller the powder particles, the faster the cooling rate. With reference to the relationship between cooling rate and particle size calculated on the assumption of Newtonian cooling [28], most of the present powder particles fall in the range of cooling rates between 10^4 and $10^6\,^{\circ}C\,s^{-1}$.

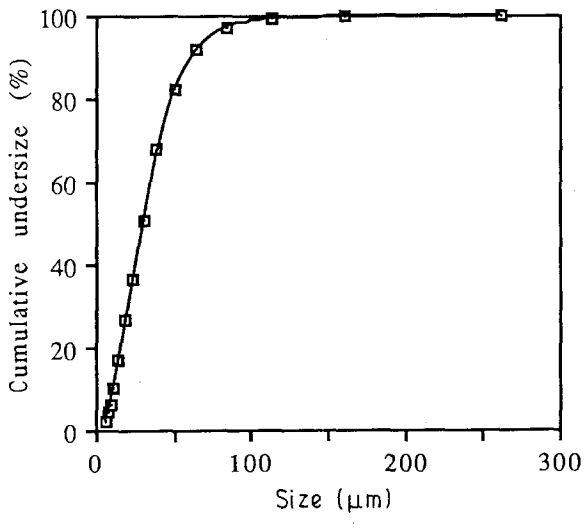

Figure 3 Size distribution of the powder. Median size = 30 μm.

Fig. 4a and b shows the general morphology of the powder as observed in the optical and scanning electron microscopes, respectively. It is clear that the finer particles tend to be rounded in shape and to aggregate. Some of the large powder particles exhibit irregular shapes, which is more likely an indication that the spheroidization of some large droplets was not completed when solidification happened, than a consequence of particle collisions [33]. For a particular alloy and under a given condition of atomizing in an inert atmosphere, there are mainly two factors governing the relation between the size and shape of powder particles. On one hand, finer particles cool at a higher rate which gives a shorter time for spheroidization. On the other, finer particles have a higher specific surface area which accelerates the spheroidization. Clearly, for the present powder, the latter factor played a major role, which agrees with the finding that spheroidization time is a fourth power function of droplet size, while solidification time is a square power function [34].

From Fig. 4c, it can be seen that many very fine particles adhere to larger particles to form satellites or agglomerates. As the satellites are nearly perfectly spheroidal, it is thought that collisions happened when the particles were almost solidified. Collisions between fully molten droplets and solidified particles were, however, occasionally observed. Fig. 4d shows the droplets enveloping more than half of the periphery of the powder particles being capped. As will be shown later, the featureless microstructure of the splat caps suggests that the particles being capped had already been chilled when the collisions occurred.

The surface of the large powder particles is not smooth, but the distinct characteristic of cellular or dendritic topography as typically seen in some other atomized powders due to final solidification shrinkage is not obvious either, Fig. 5a. Generally, finer powder particles exhibit a smoother surface, implying the tendency to the occurrence of a relatively homogeneous solidification process. A close observation by SEM at an increased magnification, however, revealed numerous protuberances on the powder particle surface with various lateral dimensions, as shown in Fig. 5b. This seems to correspond well with the results of Auger spectroscopic analysis, implying that the protuberances are possibly the products of surface reactions, that is, oxides formed during powder production. This observation has not been reported in other atomized aluminium alloy powders, but it was proved in a stainless steel powder [35].

3.4. X-ray diffraction

It is known that under the condition of rapid solidification, the solubilities of iron, molybdenum and

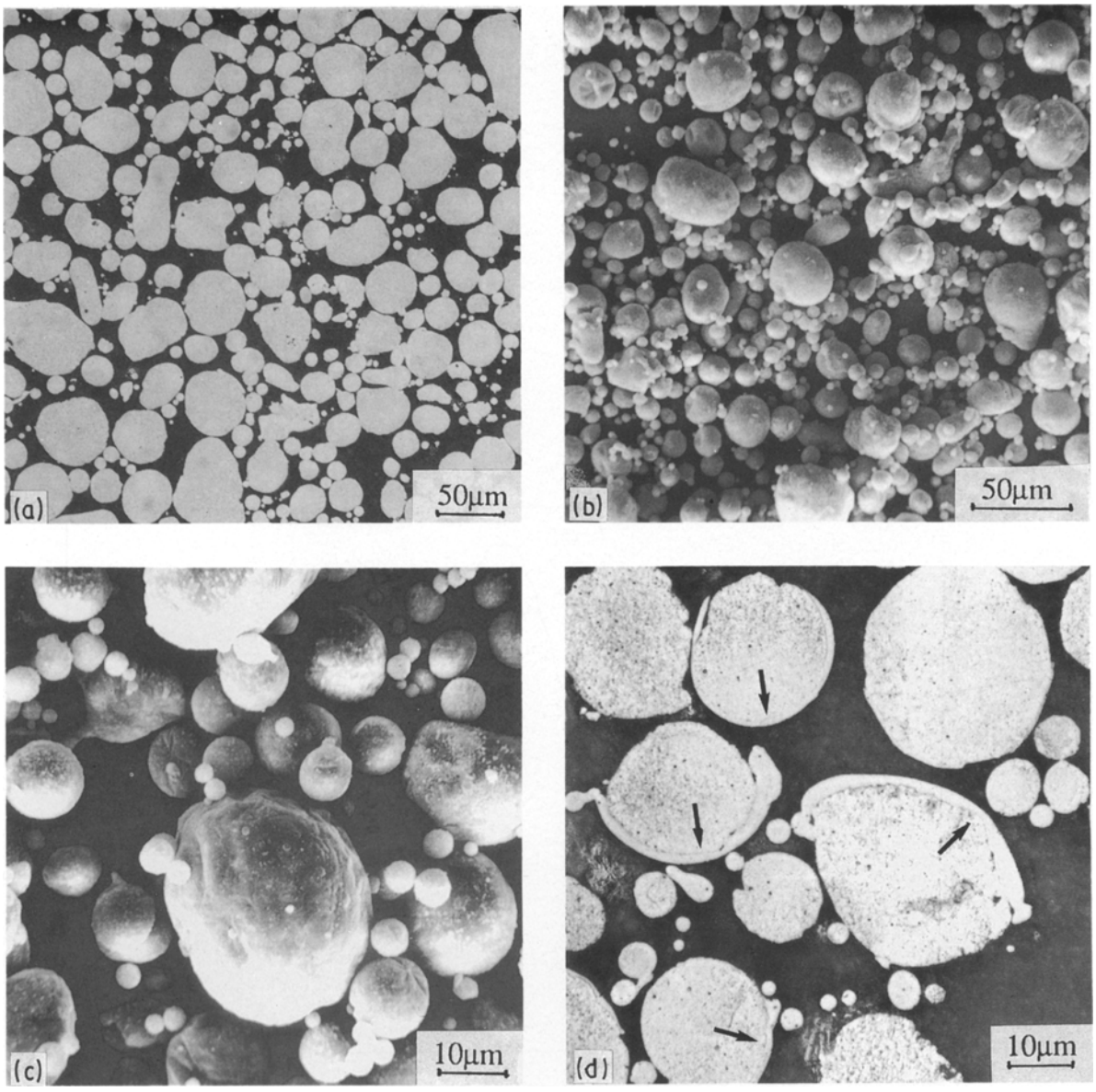

Figure 4 (a) optical and (b) SEM morphology of the powder particles, (c) adherence of very fine powder particles to large ones, and (d) collisions between molten droplets with solidified powder particles.

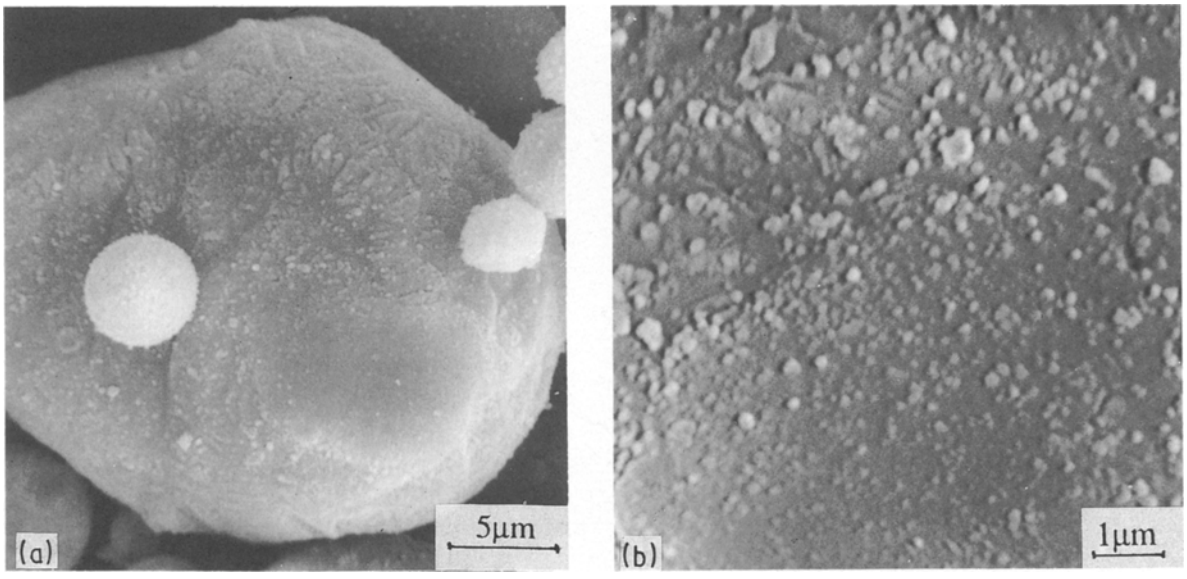

Figure 5 (a) a general view of the powder particle surface, and (b) a close inspection of the powder particle surface revealing numerous protuberances.

zirconium in aluminium can possibly be enlarged to be 240, 15 and 18 times higher than their maximum equilibrium solubilities, respectively [36]. The alteration of the lattice parameters of the α-Al matrix is often regarded as an indication of the supersaturation degree of the alloying elements involved. Fig. 6a shows the X-ray diffraction profile from the reflection plane (4 2 0) of the α-Al matrix at the diffraction angle $2\theta = 162°$. The lattice parameter was calculated to be $a = 0.40502$ nm, from the Al$K\alpha_1$ diffraction after separation from the Al$K\alpha_2$ diffraction. Due to the fact that the equilibrium solubilities of the alloying elements in the α-Al matrix at room temperature are extremely low, its lattice parameter may be taken as being equal to that of pure aluminium ($a = 0.40494$ nm at 23 °C). Based on this, a lattice strain of 0.02% can be obtained, which is of course a consequence of the rapid solidification. The increased lattice parameter of the α-Al matrix in the present quaternary alloy powder is, however, contrary to the measurement of that in the substrate side of a splat-quenched Al–8Fe binary alloy which showed a reduction in lattice parameter by 0.6% [2]. The causes for the alteration of lattice parameters in rapidly solidified aluminium alloys are very complicated, and insufficient data are currently available to give a convincing explanation of the value measured in this work. Nevertheless, the following factors can be taken into account that may contribute

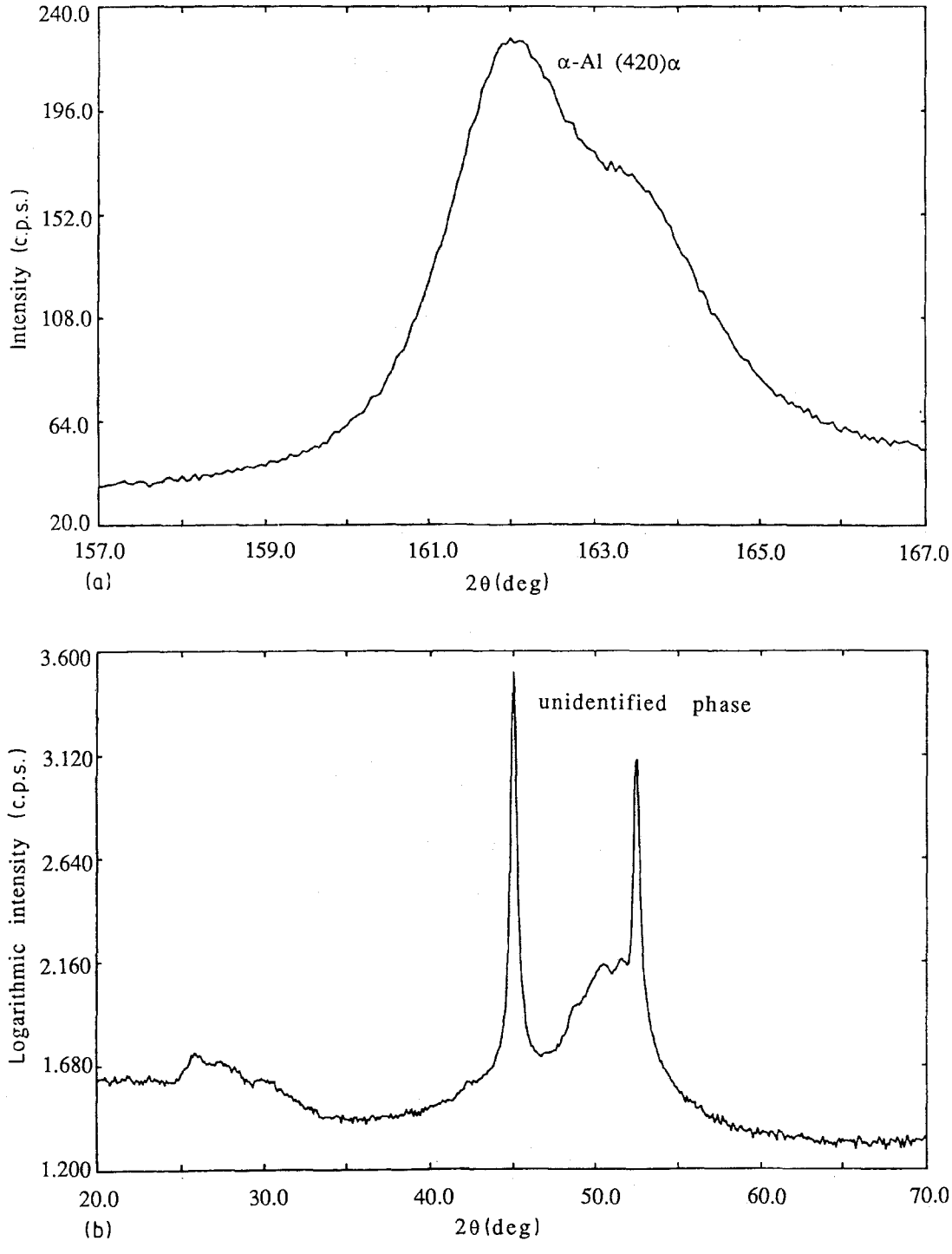

Figure 6 (a) X-ray diffraction of the matrix from the reflection plane (4 2 0), (b) X-ray diffraction of the second phase.

to the increased lattice parameter of the present α-Al matrix. Firstly, in this quaternary alloy, a substantial amount of zirconium is supersaturated in matrix, resulting in an increased lattice parameter of the α-Al matrix [37]. Secondly, the alteration of the α-Al lattice parameter is complicated by the situation of iron atoms (smaller than aluminium atoms) in the aluminium solution, which are not necessarily substitutional and can possibly be interstitial or segregated in clusters and particularly at grain boundaries [38]. The resultant value of this parameter is thus dependent to a certain extent upon the specific solidification technique employed. This is likely to be one of the causes for the significant inconsistency in the α-Al matrix lattice parameters of Al–Fe binary alloys measured by different investigators [38]. For example, Badan *et al.* used Mössbauer spectroscopy and an X-ray diffractometer to investigate the change of lattice parameter in the Al–Fe melt-spun ribbons. They found that with the increase of iron content over the range of 0.5 to 3.5 wt %, single iron atoms in substitutional solid solution decreased significantly, and the lattice parameters of the matrix, only marginally lower than that of pure aluminium, showed a tendency of increase. It was explained by a drainage effect due to the increased tendency to the growth of iron-containing intermetallics [38]. Thirdly, the cooling rate and thus the supersaturation degree of iron are relatively lower in atomized powder than those of the splat-quenched ribbon, especially close to the substrate side. The reduction in lattice parameter given by iron supersaturation in the bulk powder cannot thus be very high. Fourthly, the supersaturation level can be strongly dependent upon the size of the powder particles detected and their microstructure. In the air-cooled side of the splat-quenched Al–8Fe ribbon no significant shift or broadening of the α-Al matrix reflections was observed [2]. In the present powder, the majority of the powder has a cellular microstructure similar to the air-cooled side of the ribbon, and thus a high modification of iron to the α-Al matrix lattice parameter cannot be expected. The lattice parameter of the α-Al matrix in the present powder is not therefore merely a result of iron substitution any more which usually leads to a reduction, but a combined result of many effects involved.

An attempt was also made to identify the dispersed phases in the atomized powder using X-ray diffraction. Fig. 6b presents some recorded diffraction lines with very strong intensities. The peaks could not readily be assigned to established binary phases with stoichiometric compositions in Al–Fe, Al–Mo or Al–Zr alloys, although it has been claimed that in the equilibrium state binary compounds such as $FeAl_3$, $MoAl_{12}$ and Zr_3Al rather than new, ternary or quaternary phases are formed [37]. It is thus clear that the rapid solidification applied in the atomization of the alloy suppressed the formation of stoichiometric equilibrium phases, but produced metastable phases. Adam found from a transmission electron microscopy investigation that the very fine intermetallic phase in the microcellular structure (optically featureless) of the as-solidified Al–8Fe–2Mo powder was amorphous with an approximate composition Al(Fe, Mo) [39]. It was later confirmed in the melt-spun ribbons of the same ternary alloy by microdiffraction that the very fine intercellular phase was quasi-crystal and designated as T′ phase [40]. In the present investigation, the powder was analysed as a bulk material, and hence the peaks can hardly be considered to be generated from the quasi-crystal T′ phase because the majority of its microstructure is composed of the coarse cells containing larger dispersoids. In the cellular structure of rapidly solidified Al–Fe alloys, a new metastable phase, $FeAl_6$, has been identified [2] and confirmed extensively. The present diffraction lines did not, however, match those of this non-equilibrium phase well (the closest composition is $FeAl_2$ which might not be true). This may be largely due to the association of molybdenum with the Al–Fe intermetallic phase in the cells, which can result in a modification to the diffraction pattern. The supporting evidence for this was obtained from the X-ray mapping in the scanning electron microscope which showed a homogeneous distribution of molybdenum all over the powder particle cross sections. Diffractions from other dispersoids corresponding to zirconium-rich binary phases in the powder were not detected, in agreement with the result obtained from the splat-quenched Al–8Fe–1Zr alloy [41]. This confirms that most of the zirconium was retained in solution with a result of modifying the lattice parameter of the matrix. Zirconium was added with the intention to create additional strengthening by forming Al_3Zr; thus its precipitation from the metastable α-Al solution can be expected to occur during subsequent degassing and extrusion.

3.5. Microstructure

The microstructure of the powder was found to be very much dependent upon the size of individual powder particles. For the particles smaller than 10 μm, optical revelation of their microstructure was difficult, because it was extremely fine and rather irresponsive to etching. No coarse, primary phases in these powder particles were observable, indicating that their formation was effectively suppressed by rapid solidification. This featureless microstructure definitely corresponds to that in the substrate side of splat-quenched Al–Fe ribbons, commonly called zone A [2]. It is important to note that the size of the powder particles with entirely featureless microstructure is restricted to 10 μm, probably because of the limited undercooling in atomization and the suppressing effect of zirconium on the formation of such a microstructure [39]. As shown earlier, only 8% of the powder particles fall in this size range, and 92% are larger than 10 μm. The larger powder particles generally contain three distinct zones with discernible boundaries, which respond differently to etching and exhibit differing morphologies. Fig. 7a and b shows a typical morphology of the etched powder particle sections, as revealed by optical and scanning electron microscopy, respectively. The relative area of the three zones varies with powder particle size. Apparently, the observed microstructure in the present powder is not identical to that in the splat-quenched ribbons which optically exhibit only

two zones, A and B [2]. Characterization of the powder with such a peculiar microstructure composed of three zones is thus of interest, and reported on hereafter, while ultrafine powder particles with an entire featureless microstructure, from a practical point of view, is not the prime concern of the present work. To avoid a possible confusion with the microstructural transition in the splat-quenched ribbons of Al–Fe–X alloys, the three zones in the present powder are termed numerically in this communication, as indicated in Fig. 7.

Fig. 7a to f shows the structural transitions across powder particle sections and the characteristics of each zone revealed by optical and electron microscopy. It can clearly be seen from Fig. 7a that inside a powder particle there are dark grey regions (zone 2),

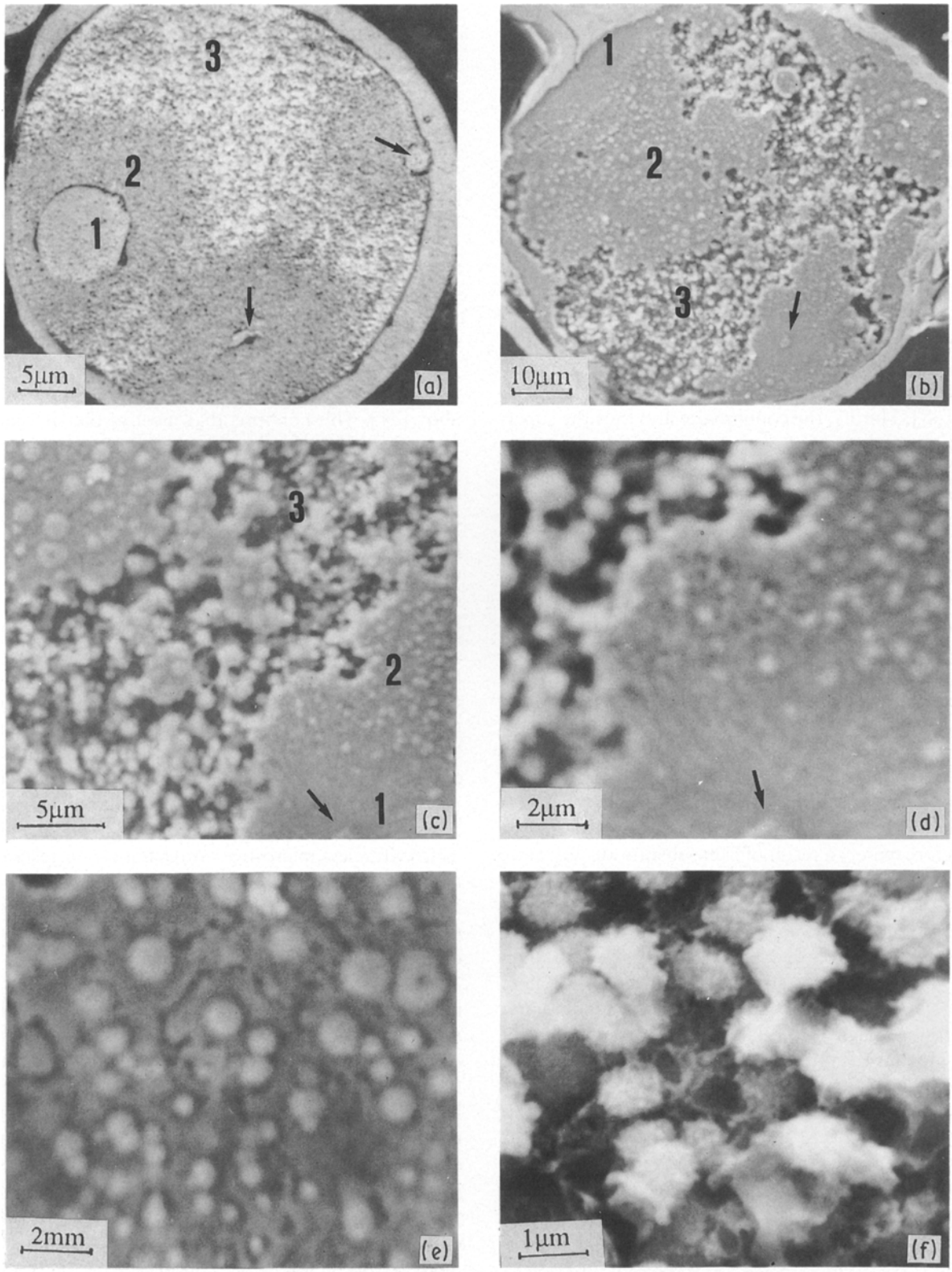

Figure 7 (a) Optical microstructure of a powder particle section, (b) SEM microstructure of a deeply etched powder particle section, (c) structural transitions across a powder particle section, (d) microstructure of zone 1 composed of a nucleus and radiating columns, (e) microstructure of zone 2 characterized by dispersed particles, and (f) cellular microstructure of zone 3 with internal particles.

each of which contains a core (zone 1) situated either at or close to the powder particle surface. The size of the cores, depending on local undercooling level, varies greatly within each powder particle and with powder particle size, ranging from 2 to 10 μm. This size range corresponds to that of the powder particles which show an entirely featureless microstructure. These cores are evidently the origins of solidification. The presence of several cores in one powder particle indicates multiple nucleation events simultaneously occurring in one liquid droplet. Their location implies that the powder particle surface, with initial oxide particles, provided the heterogeneous nucleation sites for solidification. When a core is not located at the periphery, there is a dispersoid particle in the centre, as indicated by arrows in Fig. 7b and c. This is direct evidence of heterogeneous nucleation, catalysed by the dispersoid particles that appear to be formed at the very beginning of solidification. Fig. 7d shows the details of zone 1 from which it can be seen that around this dispersoid particle, the microstructure is essentially devoid of other coarse dispersoids. This implies that the initial solidification around the nucleation sites was so rapid that the early formation of dispersoids during solidification was suppressed there. A columnar structure radiating from the dispersoid particle indicates the directional heat transfer during the formation of this zone. This heat transfer was very effective so that the decomposition in this zone during secondary cooling was completely prevented. Apparently, zone 1 in the present powder is essentially the same as zone A adjacent to the substrate in the splat-quenched ribbon, which has already been shown to be composed of very fine iron-rich particles enveloped by a microcellular aluminium matrix [3].

Of more interest is the zone 2 outside the solidification origin, which occupies a large fraction of the section area. Fig. 7a shows that this zone was also fairly resistant to etching, although numerous, fine dots could be seen optically. SEM of the heavily etched powder particle sections clearly showed the dispersoid particles protruding from the etched cross-sections in this zone, with a size increasing with the distance from the solidification origin, Fig. 7c and e. An indistinct cellular matrix structure in the region close to zone 3 was sometimes observable, see Fig. 7e. Hence, it would be misleading if this zone is regarded as being identical to the real featureless zone with extremely fine intercellular particles. Some of the dispersoids in zone 2 might be the primary phase formed at the commencement of solidification, but most of them are likely to be the products of decomposition occurring in the solid state during secondary cooling, as a result of recoalescence of the preceding solidification. It appears that the thermal recoalescence from the formation of the core decreased the undercooling of this zone to a certain extent, but insufficiently to result in cellular or dendritic solidification. It is also very likely that the releasing rate of latent heat was extremely high which did not permit the heat dissipation to the atomizing gas. Consequently, the solidified material in this zone was reheated up to a temperature where precipitation occurred. In the remaining liquid, the temperature gradient was decreased and the released latent heat substantially lowered its undercooling level, so that its solidification occurred in a different manner, leading to a clear structural transition from zone 2 to zone 3, see Fig. 7a to c and 7e to f. Clearly, zone 2 reflects an intermediate stage between the initial, instantaneous solidification and show cellular solidification; therefore, the present powder exhibits unique, multiple structural transitions, being somewhat different from splat-quenched or melt-spun ribbons of Al–Fe–X alloys, which have been subjected to extensive investigations. Of course, in a broader sense zone 2 in the present powder may be classified to belong to zone A as defined in the splat-quenched ribbon [2] so as to distinguish it from the coarse, cellular structure, if only the matrix structural size is taken into consideration.

As shown in Fig. 7, the structural transition from zone 2 to zone 3 is abrupt, and zone 3 exhibits an optically observable cellular structure with interior dispersoid particles, Fig. 8a. Cell size, depending on the rate of heat extraction during solidification, increases with rising particle size, but is typically around 1 μm. Each equiaxed cell usually contains several intercellular dispersoids. Fig. 8b and c shows the morphology of the dispersoids that are granular with a size of ~ 0.5 μm. Their presence suggests that the undercooling level in this zone was so low that high supersaturation was not possible and the liquid at solidification front was decomposed to form the intermetallic dispersoids. Back scattered mode of scanning electron microscopy revealed that the dispersoids were iron rich, but good images were difficult to be obtained because of the limited resolution of this mode. Other dispersoids were not found from the atomic number contrast. Of particular interest is to see the dendritic configuration of the dispersoids in the centre of a powder particle, Fig. 8b and c, which clearly illustrates the occurrence of a structural change from granular dispersoid to dendritic ones along with the decrease in undercooling during solidification. These dispersoids might be formed in the droplets and acted as the internal nuclei for the further solidification. The presence of the massive intercellular iron-rich dispersoid particles indicates that the matrix supersaturation in this zone cannot be very high. Except for the granular dispersoids, acicular platelets, with the typical morphology of Al_3Fe phase, were occasionally observed in a few large powder particles, (see Fig. 9), which could be attributable to accidental, inadequate cooling of a few powder particles in the atomizing chamber.

It should be mentioned that in Fig. 7a there is a peripheric rim, arising from a particle collision during atomization. The featureless structure of the rim implies that its solidification was very rapid and was not affected by the heat dissipation of the powder particle being capped. It means that the particle being capped had been chilled when the collision took place. Another factor contributing to the featureless structure of the cap is that collision provided energy to catalyse its solidification [41]. Clearly, this kind of collision, though unavoidable during atomization,

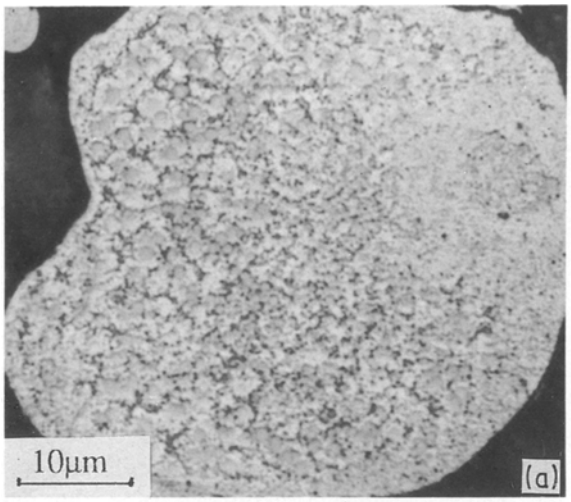

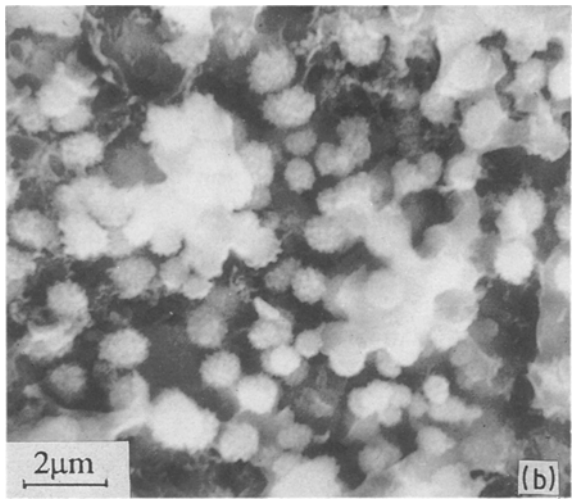

Figure 8 (a) optical microstructure of zone 3 showing cellular network of matrix with internal dispersoids, (b) and (c) SEM microstructure of zone 3 showing the size, morphology and distribution of dispersoid particles.

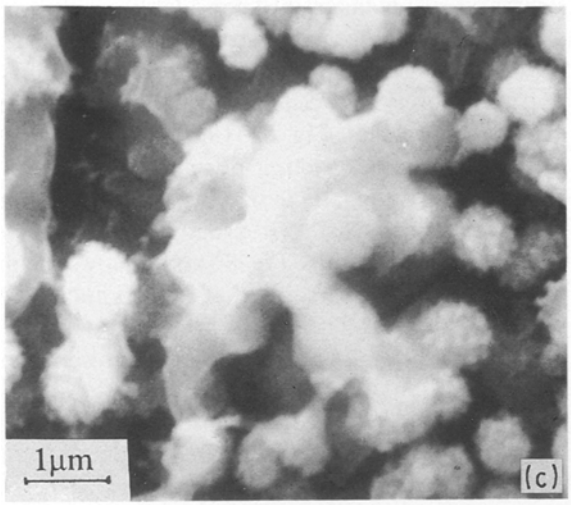

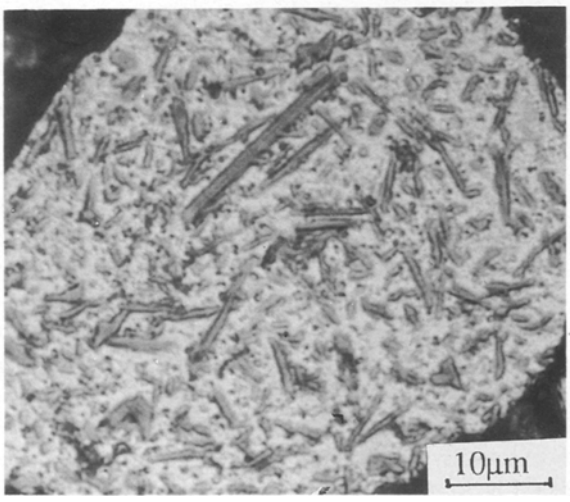

Figure 9 Needle-shaped intermetallic phase occasionally observed in some large powder particles.

results in extra microstructural transitions across powder particle sections, and thus may be unfavourable to the homogeneous properties of the material.

It is clear from the above that the inhomogeneous microstructure in the powder was caused by the varying undercooling across the powder particle sections, which resulted in the operation of different solidification mechanisms. According to the above observations, the following solidification processes occurring during the atomization of the present powder can be described. A few surface oxides or dispersoid particles first formed at the early stage of solidification. They acted as potent nuclei and solidification started around them in adiabatic manner. Further solidification proceeded very quickly in radial directions extending from zone 1 to zone 2 due to a high undercooling level and, at the same time, the release of latent heat resulted in the formation of numerous dispersoid particles in zone 2. With the proceeding of solidification and release of latent heat, the undercooling in the remaining liquid became significantly reduced, which made its solidification occur almost isothermally. A coarse cellular matrix with granular dispersoids and then dendritic dispersoids was formed at a rate depending on the rate of heat extraction from the interior to the surroundings.

3.6. Microhardness

The variation in microstructure within the powder particles and with powder particle size results in non-uniform microhardness. Fig. 9 shows the average microhardness values measured on the powder particle sections. In this test, zones 1 and 2 were impossible to distinguish in spite of the fact that a very low load was used. It should also be noted that the section area does not necessarily represent the powder particle size, but the indication is very clear that the microstructural transition in medium and large powder particles gives significant variations in hardness. Apparently, the hardness property of the individual powder particles smaller than 10 μm is excellent, but achieving such a size range at present is not feasible, especially in commercial production, although the calculated requirement of cooling rate for homogeneous solidification ($10^{12}\,K\,s^{-1}$) may be somewhat overestimated [42]. Even if such a size range was obtained, the specific surface area of the powder

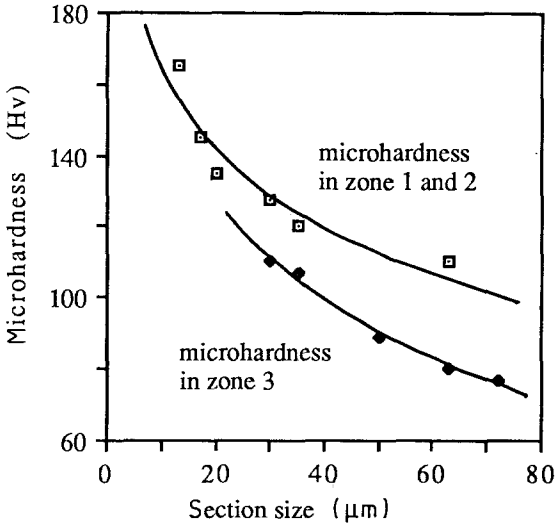

Figure 10 Variations of microhardness in the powder particle section with powder particle size.

would be greatly increased, and oxygen and hydrogen contents would accordingly rise. As a result, problems associated with proper degassing and preventing contamination would be encountered. Also, the retention of the metastable, optically featureless microstructure throughout the fabrication cycle would be a challenge. Furthermore, the embrittlement resulting from the presence of oxides in the consolidated material [43] would be an obstacle to the successful application of the alloy. If these problems are not satisfactorily solved, the final properties of the bulk material cannot be ensured. At present, therefore, pursuing such a fine size range of the powder particles, from a practical point of view, may not be necessary.

Within and between the medium and large powder particles, hardness values, however, vary significantly. This can be explained by the mechanisms including solute hardening, fine cell hardening and fine dispersion hardening which operate differently in the powder. Subsequent heating during degassing can hardly eliminate completely the differences in the hardness within and between the powder particles, and thus the uniform deformation of the powder during consolidation cannot be expected. Undeformed small powder particles in an extruded Al–Fe–Ce alloy, owing to their very high deformation resistance, have been reported [24]. The uniformity of the mechanical properties of the final engineering material will ultimately be influenced [44]. It is stressed, therefore, that narrowing the size range to minimize the non-uniformity of powder properties should be an important concern for the production of the present powder, for example, through increasing the velocity of atomizing gas, decreasing the nozzle size of melt flow, or sieving out extra large and small powder particles.

4. Conclusions

Based on the results shown above, the following conclusions have been drawn.

1. Although the present powder was atomized in nitrogen, surface oxidation still happened. Discrete oxide particles have been detected to be present as deeply as 100 nm below the surface. This, together with a high specific surface area, accounts for a relatively high oxygen content in the powder. A high reduction ratio of extrusion which can sufficiently redistribute the oxides is thus recommended to be used in consolidation in order to prevent possible failure of the material along the prior powder particle boundaries.

2. A high hydrogen content in the powder has been found, which is believed to be associated with the surface oxides and the high surface area of the powder. The necessity to degas the powder adequately is therefore emphasized, and an on-line degassing technique is proposed to simplify the procedure and to minimize the microstructural coarsening of the alloy.

3. The powder particles do not exhibit a smooth surface, and numerous protuberances are considered to correspond to the surface reaction products, consisting of discrete oxide particles.

4. An increased lattice parameter of the α-Al matrix in the powder bulk has been found, in contrast to a decreased lattice parameter in the substrate side of a splat-quenched binary Al–Fe ribbon. Several contributing factors are considered to explain the present experimental datum. X-ray diffraction lines from the dispersed phase do not match those of the metastable intermetallic phase in Al–Fe binary alloys, indicating the formation of a new, more complicated metastable phase in the present powder.

5. The cross-section microstructure of the powder particles larger than 10 μm is composed of three discernible zones: featureless core, transitional zone and cellular remainder. Their formation is a consequence of the difference in undercooling across the powder particle sections. The inhomogeneous microstructure results in significant variations of microhardness within and between the powder particles. An attempt to narrow the size distribution should, therefore, be made for obtaining a uniform deformation during subsequent consolidation and homogeneous properties of the final product.

Acknowledgements

The authors are grateful to the Centre de Recherches de Voreppe S.A., France, for the provision of the atomized powder used in this work. Thanks are also due to Ing. N. M. van der Pers, Ing. E. J. A. van Dam, Mr A. H. L. M. Klijnhout for their help with analytical work. The financial support of the Program for Innovative Research (IOP) in the Netherlands under the project (89-003, COST503) is gratefully acknowledged.

References

1. R. YEARIM and D. SHECHTMAN, *Metall. Trans.* **13A** (1982) 1891.
2. H. JONES, *Mater. Sci. Eng.* **5** (1969/1970) 1.
3. M. H. JACOBS, A. G. DOGGETT and M. J. STOWELL, *J. Mater. Sci.* **9** (1974) 1631.
4. M. DE SCANCTIS, A. P. WOODFIELD and M. H. LORETTO, *Int. J. Rapid Solidification* **4** (1988) 53.

5. J. W. ZINDEL, P. KURATH and H. L. FRASER, in "High Strength Powder Metallurgy Aluminium Alloys II", Proceedings of a TMS-AIME Symposium at the TMS-AIME Fall Meeting, Toronto, Canada, October 1985, edited by G. J. Hildeman and M. J. Koczak (The Metallurgical Society of AIME, Warrendale, Pennsylvania, 1985) p. 213.
6. S. C. JHA and T. H. SANDERS, Jr, *ibid.* p. 243.
7. Y. R. MAHAJAN, Y-W. KIM and F. H. FROES, *ibid.* p. 333.
8. L. ACKERMANN, S. DERMARKAR and J. F. FAURE, in Proceedings of the International Conference on Aluminium Technology '86, London, UK, March 1986, edited by T. Sheppard (The Institute of Metals, London, 1986) p. 698.
9. G. J. MARSHALL, *ibid.* p. 679.
10. P. J. M. CHARE and T. SHEPPARD, *Powder Metall.* **16** (1973) 437.
11. D. J. SKINNER, R. L. BYE, D. RAYBOULD and A. M. BROWN, *Scripta Metall.* **20** (1986) 867.
12. R. A. RAINEN and J. C. EKVALL, *J. Metals* **40** (May 1988) 16.
13. K. S. CHAN, in "Dispersion Strengthened Aluminium Alloys", Proceedings of a Symposium at the TMS Annual Meeting, Phoenix, Arizona, USA, January 1988, edited by Y-W. Kim and W. M. Griffith (TMS, Warrendale, Pennsylvania, 1988) p. 283.
14. M. K. PREMKUMAR, M. J. KOCZAK and A. LAWLEY, in "High Strength Powder Metallurgy Aluminium Alloys II", Proceedings of a TMS-AIME Symposium at the TMS-AIME Fall Meeting, Toronto, Canada, October 1985, edited by G. J. Hildeman and M. J. Koczak (The Metallurgical Society of AIME, Warrendale, Pennsylvania, 1985) p. 265.
15. M. A. ZAIDI and T. SHEPPARD, *ibid.* p. 367.
16. M. J. COUPER and R. F. SINGER, *ibid.* p. 199.
17. M. A. ZAIDI, J. S. ROBINSON and T. SHEPPARD, *Mater. Sci. Technol.* **1** (1985) 737.
18. J. W. ZINDEL, D. C. van AKEN, R. D. FIELD, P. KURATH and H. L. FRASER, in "Mechanical Behaviour of Rapidly Solidified Materials", Proceedings of a Symposium at the AIME Annual Meeting, New York City, New York, USA, February 1985, edited by S. M. L. Sastry and B. A. MacDonald (The Metallurgical Society of AIME, Warrendale, Pennsylvania, 1985) p. 189.
19. P. W. J. M. BOUMANS and F. J. de BOER, *Spectrochimica Acta* **30B** (1975) 309.
20. R. PRUMBAUM: *Int. Laboratory* **14** (October 1984) 44.
21. K. S. W. SING, D. H. EVERETT, R. A. W. HAUL, L. MOSCOW, P. A. PIEROTTI, J. ROUQUÉROL and T. SIEMIENIEWSKA, *Pure Appl. Chem.* **57** (1985) 603.
22. J. ESTRADA and J. DUSZCZYK, *J. Mater. Sci.* **25** (1990) 886.
23. Y-W. KIM and F. H. FROES, *Aluminium* **64** (1988) 1035.
24. W. A. BAESLACK III, K. H. HOU and J. H. DEVLETIAN, *J. Mater. Sci. Lett.* **7** (1988) 944.
25. K. H. HOU and W. A. BAESLACK III, *J. Mater. Sci.* **25** (1990) 2642.
26. J. L. ESTRADA and J. DUSZCZYK, in Proceedings of Second World Congress on Particle Technology, September 1990, Kyoto, Japan, Vol. 4 (Society of Powder Technology, Japan, 1990) p. 392.
27. L. NYBORG and I. OLEFJORD, *Powder Metall.* **31** (1988) 33.
28. K. AKECHI, Y. ODANI and N. KUROISHI, *Sumitomo Electric Technical Rev.* **24** (1985) 191.
29. A. NYLUND and I. OLEFJORD, *Int. J. Rapid Solidification* **4** (1989) 271.
30. J. L. ESTRADA, J. DUSZCZYK and B. M. KOREVAAR, *J. Mater. Sci.*, in press.
31. L. NYBORG, A. NYLUND and I. OLEFJORD, *Surface Interface Analysis* **12** (1988) 110.
32. W. S. MILLER, I. R. HUGHES, I. G. PALMER, M. P. THOMAS, T. S. SAINI and J. WHITE, in "High Strength Powder Metallurgy Aluminium Alloy II", Proceedings of a TMS-AIME Symposium at the TMS-AIME Fall Meeting, Toronto, Canada, October 1985, edited by G. J. Hildeman and M. J. Koczak (The Metallurgical Society of AIME, Warrendale, Pennsylvania, 1985) p. 311.
33. A. J. ALLER and A. LOSADA: *Powder Metall. Int.* **21** (1989) 15.
34. O. S. NICHIPORENKO, *Sov. Powder Metall. Met. Ceram.* **15** (1976) 665.
35. I. OLEFJORD and L. NYBORG, *Powder Metall.* **4** (1985) 234.
36. H. JONES, *Aluminium* **54** (1978) 274.
37. L. F. MONLDOFO, "Aluminium Alloys, Structure and Properties" (Butterworths, London, 1976) p. 282.
38. B. BADAN, M. MAGRINI and E. RAMOUS, *Scripta Metall.* **23** (1989) 2121.
39. C. M. ADAM, in "Rapidly Solidified Amorphous and Crystalline Alloys", Proceedings of the Materials Research Society Annual Meeting, November 1981, Boston, Massachusetts, USA, vol. 8, edited by B. H. Kear, B. C. Giessen and M. Cohen (North-Holland, New York, 1982) p. 411.
40. R. D. FIELD, J. W. ZINDEL and H. L. FRASER, *Scripta Metall.* **20** (1986) 415.
41. V. G. McDONNELL, E. J. LAVERNIA and G. S. SAMUELSEN, in "Synthesis and Analysis in Materials Processing: Advances in Characterization and Diagnosis of Ceramic and Metal Particulate Processing", edited by E. J. Lavernia, H. Henein and I. Anderson (TMS, Warrendale, Pennsylvania, 1989) p. 29.
42. J. P. HIRTH, *Metall. Trans.* **9A** (1978) 401.
43. R. H. BRICKNELL, *ibid.* **17A** (1986) 583.
44. M. A. ZAIDI and T. SHEPPARD, in "High Strength Powder Metallurgy Aluminium Alloys II", Proceedings of a TMS-AIME Symposium at the TMS-AIME Fall Meeting, Toronto, Canada, October 1985, edited by G. J. Hildeman and M. J. Koczak (The Metallurgical Society of AIME, Warrendale, Pennsylvania, 1985) p. 367.

Received 18 June
and accepted 26 June 1990